Materials Today Bio 14 (2022) 100255

Contents lists available at ScienceDirect

Materials Today Bio

journal homepage: www.journals.elsevier.com/materials-today-bio

Promoting mineralization at biological interfaces *Ex vivo* with novel amelotin-based bio-nano complexes

Mehrnoosh Neshatian [a,*], James Holcroft [a], Anil Kishen [a], Grace De Souza [a,c], Bernhard Ganss [a,b]

[a] Faculty of Dentistry, University of Toronto, 124 Edward St, Toronto, ON, M5G 1G6, Canada
[b] Institute of Biomedical Engineering (BME), University of Toronto, Rosebrugh Bldg, 164 College St Room 407, Toronto, ON, M5S 3G9, Canada
[c] School of Dentistry, University of Louisville, 501 S Preston St, Louisville, KY, 40202, United States

A B S T R A C T

Interfacial failure at the resin-dentin interface is a significant disadvantage of resin-based dental restoration. In this study, we created bio-inspired bio-nano complexes using the enamel protein amelotin (AMTN) or AMTN with an engineered collagen-binding site (AMTN-Col) to coat hydroxyapatite nanoparticles (HANP). The resulting nano-bio complexes, AMTN-HANP and AMTN-Col–HANP, were evaluated for their ability to promote collagen mineralization. Our study comprises three separate phases.

In phase I, developing a method for functionalizing HANP with AMTN/AMTN-Col was explored. HANP were synthesized and characterized using TEM, SAED-TEM, XRD and ATR-FTIR. The nanoparticles were functionalized with AMTN or AMTN-Col. The successful coating of the nanoparticles with the proteins was confirmed using a TEM image of immunogold-labelled samples.

In phase II of the study, the mineralization potential of the synthesized bio-nano complexes was studied using model systems consisting of simulated body fluid (SBF), polymerized collagen gels, and dentin disks prepared from human extracted molars. Mineral formation in SBF was recorded with a light scattering assay using a microplate reader on 8 replicates of each sample per study time point. Statistical analysis was performed using one-way ANOVA and the Tukey test. Significance was assigned at $P < 0.01$. The extent of mineral formation on collagen gel and remineralization of demineralized dentin was studied with SEM. Accelerated mineral formation collagen mineralization of bio-nano complexes treated samples were observed in all model systems.

In phase III of the study, the clinical utilization of AMTN/AMTN-Col coated HANP in bio-integration and enhancing the bond strength of a resin-based dental restoration and the dentin interface was investigated. The bio-nano complexes were applied as a pretreatment on dentin disks prepared from human extracted molars prior to the composite resin restoration. The micro-shear bond strength test was done on 8 samples per treatment group (a total of 32 samples). Statistical analysis on shear bond strength was performed using one-way ANOVA and the Tukey test. Significance was assigned at $P < 0.01$. Shear bond strength values indicated that pretreatment of dentin with the bio-nano complexes before adhesive application significantly improved shear bond strength.

Conclusion: We have shown that AMTN based bio-nano complexes promote mineral formation on collagenous interfaces. Our findings can be the basis of new bio-inspired, bio-nano materials that may improve dental restoration longevity by enhancing the stability and integrity of the dentin-composite resin interface.

1. Introduction

Collagen is the most abundant protein in the human body and is the building block of mineralized tissues, such as bone and teeth. Mineralized tissues usually develop within an organic matrix, such as collagen, that accommodates mineral crystals [1–3]. Dentin organic matrix is mainly made of type I collagen that serves as a structural matrix that accommodates carbonated apatite minerals. Demineralization of enamel or dentin caused by acidogenic activities of oral microorganisms can result in dental caries. Untreated caries in permanent and deciduous teeth are among the most prevalent chronic diseases worldwide [4].

Despite the advancements in preventive and restorative dentistry during the past decades, a considerable number of restorative treatments in a dental office include replacing failed fillings due to recurrent caries. The placement and replacement of dental fillings impose a substantial economic burden [5–8]. Secondary caries, defined as the development of lesions at the interface of tooth tissue and filling materials, are the primary reason for most typical direct restoration failures [9,10].

Furthermore, post-restoration dentin hypersensitivity (DH) with composite fillings is a common issue [11]. Therefore, restorative materials that can facilitate remineralization of dentin at the interface of restoration and native dentin tissue are of considerable interest since they may lead toward a more integrated interface, improved bond stability, prevent restorative failures, and prevent postoperative hypersensitivity

* Corresponding author.
E-mail addresses: Mehrnoosh.Neshatian@mail.utoronto.ca (M. Neshatian), james.holcroft@utoronto.ca (J. Holcroft), anil.kishen@dentistry.utoronto.ca (A. Kishen), Grace.desouza@louisville.edu (G. De Souza), b.ganss@utoronto.ca (B. Ganss).

https://doi.org/10.1016/j.mtbio.2022.100255
Received 13 January 2022; Received in revised form 1 April 2022; Accepted 2 April 2022
Available online 6 April 2022

[12,13].

Many non-collagenous proteins, such as phosphorylated proteins, proteoglycans, and glycoproteins, play an essential role in regulating and controlling mineral formation [14–16].

Amelotin (AMTN) is an enamel protein secreted specifically during the maturation stage of enamel formation [17]. Previous studies in our lab have shown that overexpression of AMTN in a transgenic mouse model led to disorganized but highly compact enamel [18]. In contrast, the AMTN knockout mouse showed hypo-mineralized enamel [19]. We have also demonstrated that AMTN has a high affinity to hydroxyapatite (HA) [20]. HA, the most stable calcium phosphate mineral, makes up the bulk of human bone and tooth structure. It is also one of the most biocompatible materials used in mineralized tissue regeneration [21–23]. HA crystals in enamel, dentin, and bone are in the nanometer range, with enamel crystals being 10 to 100 times larger than those in dentin and bone [24]. Recent studies have shown AMTN promotes mineral formation in mouse osteogenic cells (MC3T3-E1) *in vitro* after 10 days. Further, collagen membranes, with or without recombinant human AMTN, were shown to promote bone healing in rat calvaria defects in about 8 weeks. Danesi et al. have shown AMTN can promote nanoscale uniaxial growth of hydroxyapatite along Amelogening nanoribbons. While these studies brought a profound understanding of AMTN's role as the promoter of mineralization and further confirmed the protein's ability in promoting mineralization in different settings, the clinical translation is vague, particularly for interfacial biomineralization where the challenges are unique. For example, long mineralization time would not be feasible in non-cell-mediated remineralization of dentin. The low density of the mineral formation evident in the abovementioned studies could be another concern. Therefore, this study was designed to address these issues by engineering AMTN into a bio-nano complex that can promote mineralization in a clinically reasonable time frame and shed light on the potential for clinical application.

In this study, we have used a bio-inspired approach to harness the maximum ability of AMTN in promoting mineral formation by mimicking the AMTN native microenvironment. In the native tissue, AMTN is secreted into a matrix made of nano-sized HA. Therefore, we have coated the protein on HANP to simulate the native microenvironment. Furthermore, we have engineered a collagen-binding peptide derived from DMP-1 at the C terminus of the protein [25]. We studied the effect of the collagen-binding peptide on the mineral-promoting property of the protein. This peptide will be of interest in future collagen biomineralization studies.

In this study, we investigated the following 3 main objectives. First, to develop a method to functionalize the HANP with AMTN/AMTN-Col. Second, to study the mineralization potential of the synthesized bio-nano complexes using model systems consisting of simulated body fluid (SBF), polymerized collagen gels, and dentin disks prepared from human extracted molars, and third to investigate the clinical utilization of AMTN/AMTN-Col coated HANP in bio-integration and enhancing the bond strength at resin-dentin restoration.

We hypothesized that AMTN/AMTN-Col–coated HANP promotes mineral formation on collagen-based matrices and may improve resin-dentin bond strength.

2. Methods and materials

2.1. Recombinant human protein production

N-terminally 6 × His–tagged recombinant human AMTN and modified AMTN with an engineered collagen-binding site (AMTN-Col) at the C-terminus was used in this study. The collagen-binding site with a specific affinity to N-telopeptide regions of type I collagen is made of nine amino acids (DSESSEEDR) and was derived from dentin matrix protein 1 (DMP1) [25]. The proteins were expressed in *Escherichia coli* (pET-15b expression system, Novagen, Merck, Darmstadt, Germany), purified on a Ni-NTA agarose column (Qiagen, Valencia, CA, USA), and eluted with imidazole (Fig. 1). The eluted protein was then dialyzed four times against 10 mM Tris (pH 7.4) and was sterilized by filtration (0.22 μm Millex-GV Filter, Millipore Sigma.

2.2. Synthesis procedure of HANP

HANP was prepared as described previously [26]. Briefly, 100 mL of $CaCl_2$ (0.01 mol/L) and 100 mL of $(NH_4)_2HPO_4$ (0.006 mol/L) solutions were mixed, and the pH was adjusted to between 3.0 and 3.5 with 0.1 M HCl solution. Next, 100 mL of 20% glucose solution in water was mixed with 1.5 g of NaOH, and the pH was adjusted to 12.0 to 12.5 with 1 M NaOH. The mixed solution of $CaCl_2$ and $(NH_4)_2HPO_4$ was added drop by drop into the alkaline glucose solution with stirring, leading to the instant formation of HANP. The HANP suspension was centrifuged at 4000×*g* for 10 min to make a pellet of the synthesized material. The HANP pellet was then washed five times with deionized distilled water and centrifuged at 4000×*g* for 10 min to remove unreacted material. The pellet was then placed in a dry incubator at 37 °C for 1 week to dry completely. Dried HANP was ground using a mortar and pestle to obtain a very fine homogenous powder. To image HANP with a transmission electron microscope (TEM), a 1 wt% HANP solution in 100% ethanol was prepared and sonicated (Branson 2510, Thermo Fisher Scientific Inc., MA, USA)) for 4 h to form a homogenous suspension. 1 μL of HANP suspension was placed on a carbon-coated TEM grid, air-dried at room temperature and imaged with TEM and TEM-selected area electron diffraction (SAED) (TEM, FEI Tecnai 20, OR, USA). Attenuated total reflection–Fourier transform infrared spectroscopy (ATR-FTIR) (Nicolet iS50 FTIR, Thermo Fisher Scientific Inc., MA, USA) was performed at a 4 cm–1 resolution the wavenumber range of 4000 cm−1 to 400 cm–with 16 co-added scans for samples and background. The crystallinity of the synthesized HANP was studied using an x-ray powder diffraction (XRD) (XRD system whose primary components are a PW 1830 HT generator, a PW 1050 goniometer, PW3710 control electronics, and X-Pert system software, Philips, Amsterdam, Netherlands) operated with a Cu tube (wavelength Kα1 = 1.540562), at 40 kV and 30 mA with a step size of 0.02° from 20 to 55 2θ range. All the characterizations were done in triplicates.

2.3. Coating of HANP with AMTN/AMTN-Col and immunogold labelling

To coat HANP with AMTN/AMTN-Col, a solution of AMTN/AMTN-Col in 10 mM Tris at pH 7.4 and a solution of 1 wt% HANP in 100% ethanol was prepared. In a routine experiment, a 1 wt% HANP solution was prepared by mixing 0.01 gr of HANP and 1 mL of 100% ethanol. The mixture was then sonicated for 4 h in an ultrasonic bath (Branson 2510, Thermo Fisher Scientific Inc., MA, USA). To make the nano-bio complexes, 10 μg of AMTN/AMTN-Col in 10 mM Tris solution and 1 μL of 1 wt% HANP solution was mixed.

Immunogold labelling was performed by loading nickel grids with AMTN/AMTN-Col–coated HANP. This was done by placing 2 μL of the protein-coated HANP suspension directly on carbon-coated nickel grids (Electron Microscopy Sciences, PA, USA). Six replicates of each treatment group were made, 3 for the study group and 3 for the reference. Subsequently, the loaded grids were used in a standard immunogold-labelling

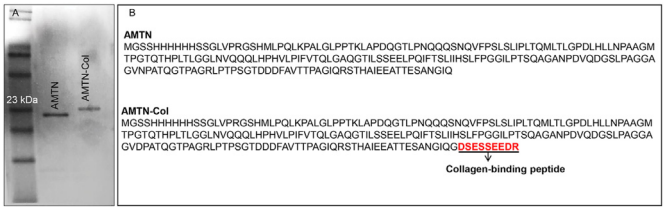

Fig. 1. (A) Coomassie blue-stained 15% SDS/polyacrylamide gel of recombinant human AMTN and AMTN-Col expressed in E. Coli bacteria and affinity purified. (B) The amino acid sequence of AMTN and AMTN-Col.

procedure [27]. Briefly, grids were air-dried, fixed with 4% paraformaldehyde and 1% glutaraldehyde for 30 min at room temperature, and blocked with 4% bovine serum albumin for 1 h at room temperature. The blocked samples were incubated with a solution containing a 1:10 dilution of primary anti-AMTN antibody in phosphate-buffered saline (PBS) (experimental groups) or PBS only (reference group) overnight at 4 °C. The following day, samples were incubated with secondary 15 nm–diameter gold particle–conjugated goat anti-rabbit IgG (H&L EM-grade 15 nm, Electron Microscopy Sciences, PA, USA) for 1 h at room temperature; samples were then washed four times each with PBS for 10 min, washed two times with distilled deionized water, and air-dried. To remove unreacted materials, samples were washed four times for 10 min each with PBS between all the steps mentioned above. Once the samples dried, they were imaged with TEM. In this study, the reference samples were only treated with the secondary antibody to investigate for nonspecific binding of the secondary antibody to the sample.

2.4. In vitro mineralization assay

A modified simulated body fluid (SBF) buffer was prepared as described [28]. The buffer contained 15 mM K^+ (KCl 99.5% AnaLaR, BDH Inc., Toronto, Canada), 0.8 mM Mg^{2+} ($MgCl_2 \times 6H_2O$, Sigma), 10 mM HCO_3^- ($NaHCO_3$, Sigma), 3 mM Ca^{2+} ($CaCl_2 \times 2H_2O$ analytical reagent AnaLaR), 1.8 mM phosphate (Na_2HPO_4, Sigma S7907), 50 mM HEPES (biotechnology grade, Bioshop Canada Inc., Burlington, Canada), and 140 mM Na^+ (NaCl reagent grade, Bioshop Canada Inc., Burlington, Canada; $NaHCO_3$, Sigma). After adjusting the pH to 7.4 with 1 N NaOH, the buffer was filtered (0.22 μm Millex-GV Filter, Millipore Sigma, Darmstadt, Germany). Biomineralization kinetics was studied using a microplate reader according to a protocol previously developed in our lab [20]. Briefly, 0.05 μg/μL of AMTN/AMTN-Col, AMTN/AMTN-Col–coated HANP, or an equal volume of 10 mM Tris or HANP in Tris was incubated with the SBF. The buffer was added to wells of a sterile non–tissue culture 96-well polystyrene plate (200 μL per well), with 8 replicates of each treatment group per time point, and incubated at 37 °C in a humidified incubator. The turbidity of the solution was measured, and the extent of turbidity was equated with mineral formation. The light-scattering measurements were performed in a microplate reader (Multiskan FC, Thermo Fisher Scientific Inc., MA, USA) at 540 nm after 30 min, 72 h, and 120 h of incubation. Using one-way analysis of variance (ANOVA) and the Tukey test, significance was assigned at $P < 0.01$. At the end of the experiment, the liquid inside each well was aspirated; wells were washed with deionized water and air-dried in a fume hood. Half of the dried samples were coated with 3 nm of titanium and imaged with scanning electron microscopy SEM (FlexSEM 1000, Hitachi, Japan). The other half were imaged with TEM.

2.5. Collagen mineralization

A total of 1 mL of a type I collagen solution (3 mg/mL; TeloCol, Advanced BioMatrix, Carlsbad, CA, USA) was mixed with an ice-cold proprietary neutralizing solution at a volume ratio of 1:9 as recommended by the manufacturer. A total of 9 collagen gel was made (3 replicates for each treatment group). Briefly, 100 μL of the mixed solution was placed on glass coverslips and placed in a humidified incubator at 37 °C for 3 h to complete polymerization. The polymerized collagen gel was treated with a volume of AMTN/AMTN-Col–coated HANP that contained 10 μg of protein (typically around 5 μL of the protein-coated HANP solution) or an equal volume of HANP in 10 mM Tris as reference. Samples were placed in a 37 °C incubator until the treatment solution was fully absorbed into the collagen gel. Treated samples were incubated in SBF for 30 min and 24 h, dehydrated using an increasing concentration of ethanol, and then imaged and characterized by SEM, ATR-FTIR, and XRD.

2.6. Dentin demineralization

Third molars extracted from humans were collected under a protocol approved by the Health Sciences Research Ethics Board of the University of Toronto (Reference #34892). Caries-free, 0.5-mm thick coronal dentin slices were prepared using a low-speed diamond saw using water as a coolant. Six dentin sections were collected in an area excluding superficial enamel and away from the pulp chamber. These dentin disks were divided into 2 groups with 3 samples each and demineralized with 0.5 M EDTA for 3 and 4 days. To confirm complete mineral removal, demineralized dentin sections were embedded in optimal cutting temperature (OCT) compound (Tissue-Plus™ O.C.T. Compound, Thermo Fisher Scientific Inc., MA, USA) and were sectioned using a cryostat (Leica Microsystems CM1850, Germany). These sections were then stained for mineral using the von Kossa staining protocol [29]. Briefly, dentin sections were rinsed with several changes of distilled water, followed by incubation with 1% silver nitrate for 30 min under UV light. Dentin sections were then rinsed with several changes of distilled water. Unreacted material was removed by washing with a 5% sodium thiosulfate solution for 5 min, followed by rinsing with several changes of distilled water. Finally, the dentin sections were dehydrated with graded ethanol and cleared in xylene. Coverslips were placed on the sections with the aid of mounting media. These samples were then imaged using a light microscope.

2.7. Dentin remineralization

A total of 18 dentin disks were made, totally demineralized with 0.5 M EDTA, and washed several times, followed by immersion in water for 4 days to remove the EDTA. Dentin specimens were blotted using Kimwipes. Dentin disks were then divided into 3 groups with 6 samples in each group. Each group was treated with a volume of AMTN/AMTN-Col–coated HANP containing 10 μg of protein (in a routine experiment, this would be around 5 μL of the protein-coated protein HANP solution) or an equal volume of HANP in 10 mM Tris as reference. Samples were placed in a 37 °C incubator until the treatment solution was fully absorbed. Treated samples were incubated with SBF for 30 min and 24 h. Three samples in each treatment group dried using an increasing concentration of ethanol and were characterized by SEM, ATR-FTIR, and XRD. The other 3 samples were sonicated for 2 min before dehydration and the SEM sample preparation procedure.

2.8. Micro-shear bond strength test

Dentin sections were prepared as described above and demineralized for 15 s with 35% phosphoric acid gel (Universal Etchant Etching Gel, 3 M, USA), followed by rinsing with running water for 15 s. Excess water was removed using Kimwipes. Then, dentin specimens were either treated with AMTN/AMTN-Col–coated HANP or HANP alone or did not receive any treatment. Treated samples were placed in a 37 °C incubator for 2 h. Once there was no liquid visible on the surface of the treated samples, they were rinsed with 1 mL of distilled water for about 10 s to remove non-diffused reagents. All specimens were then bonded as follows. Briefly, two coats of adhesive (Adper Adhesive, 3 M, USA) were applied with a micro-brush (Disposable micro applicator, Shintop, China) and gently agitated using the micro-brush tip for 15 s. The adhesive was air-dried gently to be thinned for 5 s, followed by light activation for 20 s at a 1-mm distance using a third-generation light-emitting diode (LED) with a power of 1200 mW/cm^2 (LED- YS-B Orthodontics Led Curing Light, Smart Curing Light, China). Subsequently, dentin specimens received a composite resin restoration (Filtek Supreme Ultra Flowable A4 shade, 3 M, USA), using a matrix of perforated pasta (Furadinho, Pastifício Santa Amália, Machado, Minas Gerais, Brazil) with the height of 1 mm. The composite was then light-activated using an LED source for 20 s. To remove the pasta matrix, it was softened by immersion in SBF for 2 h. This was done to avoid applying extra tension to the post while removing

the pasta mould. Eight composite posts were made for each experimental group, a total of 32 samples. All dentin specimens were stored in SBF for 5 days following composite resin bonding. A micro-shear bond (μSB) test was performed using a universal testing machine (Instron 4301, MA, USA) with a wire loop [30].

A shear force was applied to each specimen at a crosshead speed of 0.5 mm/min with a thin wire (0.2 mm aesthetic ligature Cr–Ni wire, Morelli, Brazil) that was looped around the resin cylinder until failure occurred. Bond strength values were obtained by dividing the failure force by the surface area of the composite posts. Statistical analysis on shear bond strength was performed using one-way ANOVA and the Tukey test. Significance was assigned at $P < 0.01$.

2.9. Statistical analysis

All statistical analysis was performed using Graph Pad Prism 8.4.2 (GraphPad Software, La Jolla, CA, USA). Statistical analysis on *in vitro* mineralization assay and shear bond strength was performed using one-way ANOVA and the Tukey test. Significance was assigned at $P < 0.01$ (***P < 0.001, ****P < 0.0001).

3. Results

3.1. HANP characterization

TEM images of synthesized HANP showed that they were rod-shaped, between 100 and 150 nm long and between 20 and 70 nm wide (Fig. 2A). Clear ring-dot patterns in the TEM-SAED confirmed the high crystallinity of these synthesized particles (Fig. 2B). XRD results indicated that the diffractions from (002), (211), (202), (310), (222), (213), and (004) planes of the synthesized HANP were located at 26.05°, 31.95°, 34.01°, 39.68°, 47.56°, 49.45°, and 53.18°, respectively, which was in accordance with the standard data of the Joint Committee on Powder Diffraction Standards (JCPDS) Card No. 09–0432 [26]. Hence, it confirmed that the synthesized material was composed of HANPs (Fig. 2C). ATR-FTIR spectra displayed a peak at 1035 cm^{-1}, which is associated with the stretching vibrations of P═O. Peaks at 1094 cm^{-1}, 567 cm^{-1}, and 605 cm^{-1} are the bending vibrations of P–O in PO_4^{3-}. The broad absorption centered at 3328 cm^{-1} is due to the stretching and bending vibrations of absorbed water. Additionally, the weak bands at 1422 cm−1 and 1456 cm−1 are attributed to CO_3^{-2}, which is likely due to adsorbed CO_2 from the air during the characterization (Fig. 2D) (22).

3.2. Immunogold labelling

TEM images of immunogold-labelled samples were acquired to investigate the effectiveness of the coating procedure. Gold nanoparticles presented as dark black dots in TEM images showed successful conjugation of AMTN/AMTN-Col on HANP (Fig. 3A and B). In contrast, control samples that had only been processed with the secondary gold antibody (Fig. 3C and D) did not show any gold nanoparticles. Accordingly, this confirms that the secondary antibody did not bind non-specifically to the HANP or to the grid. These results confirmed the successful coating of HANP with AMTN/AMTN-Col.

3.3. In vitro mineralization assay

The AMTN/AMTN-Col–coated HANP and proper reference, HANP in tris buffer, AMTN, AMTN-Col, and tris buffer only, were incubated in modified SBF to investigate the kinetics of mineral formation, as described earlier. Experimental groups containing AMTN/AMTN-Col–coated HANP showed significantly higher light-scattering values in as low as 30 min compared to all other groups indicated by the higher turbidity (Fig. 4). Wells containing AMTN/AMTN-Col or HANP solely also showed turbidity, albeit to a significantly lower density. Furthermore, results presented in Fig. 4 suggested enhanced mineral promoting ability of the protein once coated on HANP evidenced by the mineral density formed in the presence of the bio-nano complexes to the one produced in the presence of AMTN/AMTN-Col solely. Wells that did not contain the proteins or HANP remained clear during the study, demonstrating that the values obtained from light scattering were only associated with the mineral formation and not the nonspecific precipitation of SBF. SEM images of the samples also showed the needle-shaped crystals of these precipitates compared to the amorphous form of sparse depositions in protein-free, and HANP only controls (Supplementary material Figure S1). These findings further confirmed the enhanced mineralization potential of AMTN/AMTN-Col once coated on HANP.

3.4. Collagen mineralization

To study the mineral-promoting capacity of AMTN/AMTN-Col–coated HANP on collagen, we used polymerized collagen gel as a model system. Mineral formation on the polymerized collagen treated with AMTN/AMTN-Col–coated HANP was visible even to the naked eye as a dense white ring on the collagen localized to the treatment area in as little as 30 min. In contrast, the HANP treated collagen gel showed a

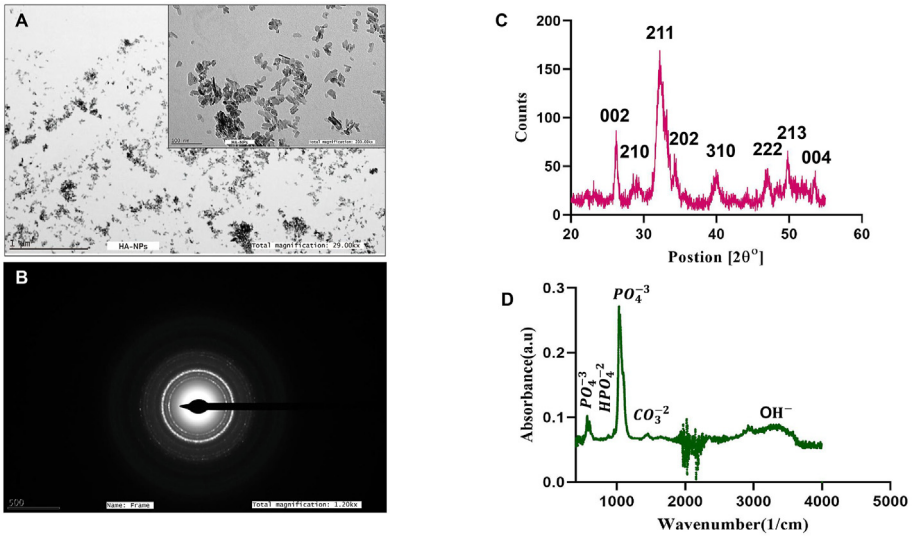

Fig. 2. HANP characterization. (A) TEM image. (B) SAED pattern. (C) XRD pattern. (D) ATR-FTIR spectra.

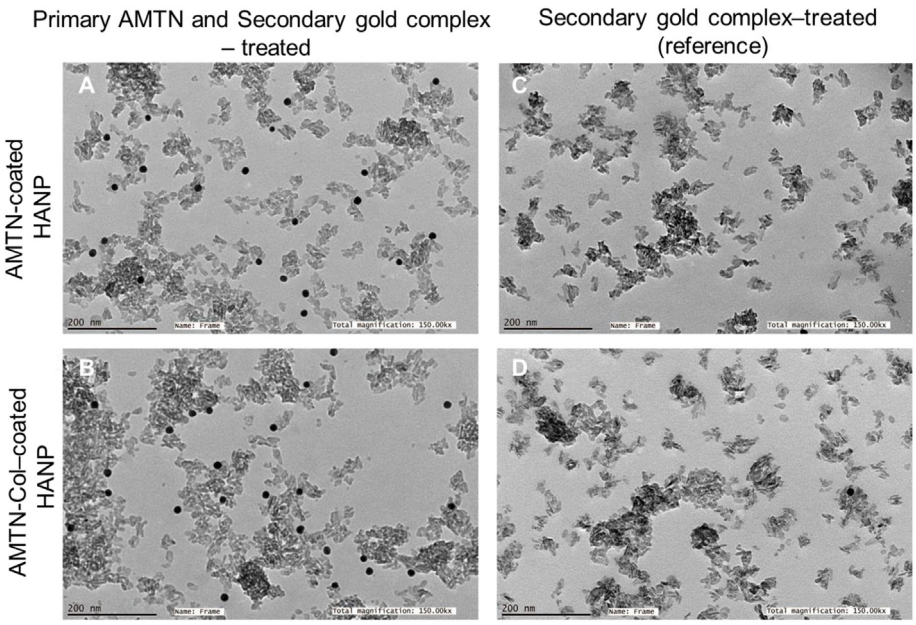

Fig. 3. TEM image of immunogold-labelled samples. (A, B) AMTN/AMTN-Col coated HANP treated with primary AMTN antibody, and secondary gold antibody (C, D) AMTN/AMTN-Col coated HANP treated with only secondary gold antibody (Control).

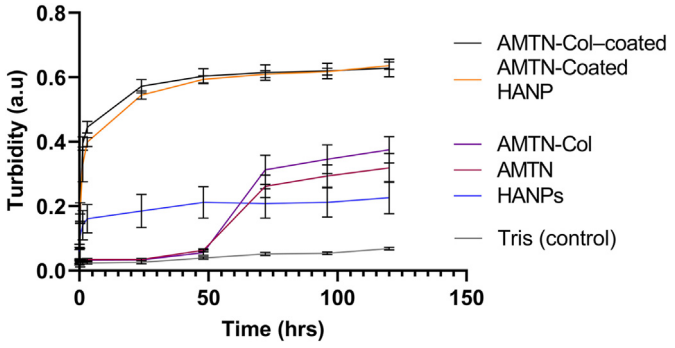

Fig. 4. Light-scattering plots of mineralization buffer–containing 0.05 μg/μL of AMTN/AMTN-Col, AMTN/AMTN-Col–coated HANP, or an equal volume of 10 mM Tris or HANP in Tris was incubated with SBF as labelled. Data are presented as mean ± standard deviation. * Indicates significantly different from other groups at every time point (***$P < 0.001$, size = 8 per group).

faded white ring (Fig. 5A), indicating a higher density of mineral formation in bio-nano complexes treated samples. SEM of these samples also confirmed a significantly denser mineral formation on samples treated with AMTN/AMTN-Col–coated HANP. Moreover, collagen treated with HANP suspension alone showed several cracks after 1 day of SBF incubation within the mineral layer, suggesting mineral layer detachments from the collagen gel. However, the mineral layer in AMTN/AMTN-Col–coated HANP samples seemed to be a homogeneous integrated layer with the collagen scaffold underneath (Fig. 5B). ATR-FTIR spectra showed a decrease in amide bond I and II peaks and an increase in phosphate peaks for all samples after 30 min and 24 h of SBF incubation compared to untreated collagen (Supplementary material Figure S2A). XRD spectra showed peaks associated with 002, 210, 211, and 222 diffraction planes in AMTN/AMTN-Col–coated HANP samples, whereas, in HANP only-treated samples, only the 211 band was present. Since the XRD signals solely depend on the absorbent's crystalline phase, these results further suggested that AMTN/AMTN-Col–coated HANP-treated specimens resulted in more crystalline mineral formation (Supplementary material Figure S2B).

3.5. Dentin mineralization

Human molar dentin slices were demineralized, as confirmed by von Kossa staining (Supplementary material S3). SEM images of samples treated with AMTN/AMTN-Col–coated HANP showed a larger and more homogeneous sheet of mineral formed on dentin and inside dentinal tubules compared to specimens treated with HANP alone (Fig. 6). Similar to collagen remineralization results, ATR-FTIR spectra of remineralized dentin showed a decrease in amide bond I and II peaks and an increase in phosphate peaks for all treatment groups after 30 min and 1 day of SBF incubation compared to nontreated dentin specimens (Supplementary material Figure S4A). This observation further confirmed mineral formation on demineralized dentin. XRD spectra showed peaks associated with 002, 210, and 211 diffraction planes in AMTN/AMTN-Col–coated HANP samples, whereas, in the HANP-treated sample, the 002 peak was the only peak present. XRD results indicated that AMTN/AMTN-Col–-coated HANP-treated samples resulted in more crystalline mineral formation (Supplementary material Figure S4B). The occurrence of excessive cracks in HANP only–treated specimens was found similar to the findings in Section 3.4. The loose attachment of the mineral sheet to the matrix underneath in the HANP only–treated samples was further confirmed by SEM images of the sonicated specimens, where disruption of the mineral layer homogeneity and its partial detachment was visible. In contrast, specimens treated with AMTN/AMTN-Col–coated HANP did not show any significant morphological changes after sonication (Fig. 6).

3.6. Micro-shear bond strength

Using a previously employed μSB strength test [30,31], the mean μSB strength values were compared among all groups. Mean μSB strength values were significantly higher in the group treated with AMTN/AMTN-Col–coated HANP compared to HANP only–treated samples and to untreated samples ($P < 0.01$) (Fig. 7A). The failure modes in both AMTN-coated HANP-treated samples and AMTN-Col–coated HANP-treated samples suggest cohesive fracture within the adhesive and/or the composite layer (Fig. 7B). In contrast, dentinal tubules were visible in nontreated samples (Fig. 7B), indicating adhesive fracture between the adhesive and the dentin. In HANP-treated samples, residual

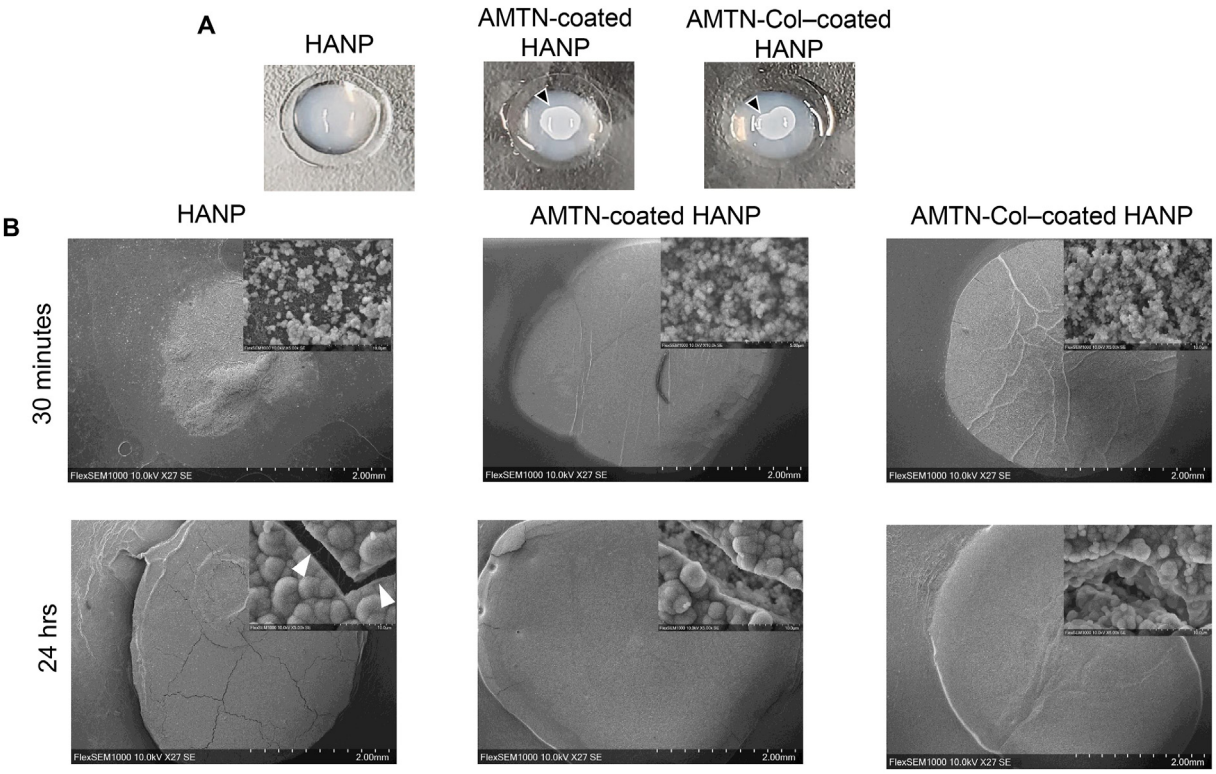

Fig. 5. (A) Image of collagen type I treated with AMTN-coated HANP, AMTN-Col–coated HANP, and HANP alone (reference) and incubated in SBF for 24 h. Arrowheads indicate visible mineral formation in AMTN-coated HANP, AMTN-Col–coated treated group compared to HANP only treated group. (B) SEM images of collagen treated with HANP, AMTN-coated HANP, and AMTN-Col–coated HANP incubated with SBF for 30 min and 24 h. The arrowhead points toward the cracks where collagen fibers are visible underneath. Indicating a possible detachment of the mineral layer from the collagen gel in HANP only treated samples.

adhesive (shown by asterisks in Fig. 7B) was visible, indicating a mixed fracture that was predominately adhesive failure between the adhesive and the dentin.

4. Discussion

In the current study, AMTN/AMTN-Col–coated HANP promoted mineral formation in SBF and were effective in promoting the mineralization of both collagen and dentin models. It was also shown that these bio-nano complexes have the potential to enhance dentin-resin μSBS significantly and may, therefore, have potential in developing future clinical applications in restorative dentistry. Therefore, our initial hypothesis that AMTN/AMTN-Col–coated HANP promotes mineral formation on collagen-based matrices and may improve resin-dentin bond strength is accepted.

Synthetic HA is widely used in tissue regeneration due to its high biocompatibility and similar

crystallinity to the minerals in native mineralized tissue [21–24]. Additionally, the native microenvironment where AMTN is expressed during the maturation stage of enamel formation is made of HANP crystals that make up the enamel rods and prisms. Therefore, in this study, we coated AMTN and AMTN-Col onto HANP to harness the maximum mineralization potential of AMTN and AMTN-Col by mimicking their native microenvironment.

The affinity of AMTN to HA is comparable to that of amelogenin, the most abundant enamel protein [20,32]. AMTN binding to HA may induce conformational changes to the protein structure, which may affect AMTN function. Previous experiments have shown that AMTN expression coincides with the expression of proteases, such as KLK4, in enamel. The potential structural changes of AMTN as a result of binding to HA might reduce its susceptibility to cleavage. Similar effects have been reported for certain salivary proteins that resist proteolytic cleavage due to strong binding to HA [33,34]. In addition to such changes in susceptibility to proteolytic cleavage, binding to HA may also alter the mineral-promoting activity of AMTN. Therefore, we investigated SBF mineralization in the presence of the bio-nano complexes with proper controls to determine whether AMTN/AMTN-Col–coating on HANP enhances the protein's mineral-promoting activity. The kinetics of mineral formation was studied using a monochromator-based UV/Vis microplate reader. This is a conclusive yet straightforward technique to study the kinetics and extent of mineral formation. We found that the measured turbidity as a result of mineral formation was almost two times higher and much faster in the presence of AMTN/AMTN-Col–coated HANP as compared with AMTN/AMTN-Col or HANP alone (Fig. 4). These results further confirmed the enhanced mineral-promoting effect of AMTN/AMTN-Col once coated on HANP. Our results also coincide with previous studies that have shown that AMTN promotes mineral formation from a supersaturated calcium phosphate solution [20] and also induces phase transformation of amorphous calcium phosphate to HA crystals *in vitro* [35]. It should be highlighted that AMTN is an enamel-specific protein and does not have any known collagen-binding sites. Here, we have integrated the DMP1 collagen-binding site into the C-terminus of AMTN [25]. While future experiments are required to assess the affinity of this engineered collagen-binding site to HA, we did not find any synergetic effect between the collagen-binding site and the mineralization capacity of AMTN.

Next, we investigated the mineralization of collagen *in vitro*. A fully protected collagen, either by the resin or by the mineral, at the dentin-restoration interface is critical in preventing restoration failure. Several studies have shown that collagen hydrolysis at the hybrid layer has a detrimental impact on the longevity of the restoration regardless of the bonding system [36]. Since minerals can protect collagen from hydrolysis [37], we have used polymerized collagen as a model system to study the mineral-promoting properties of AMTN/AMTN-Col–coated HANP. As

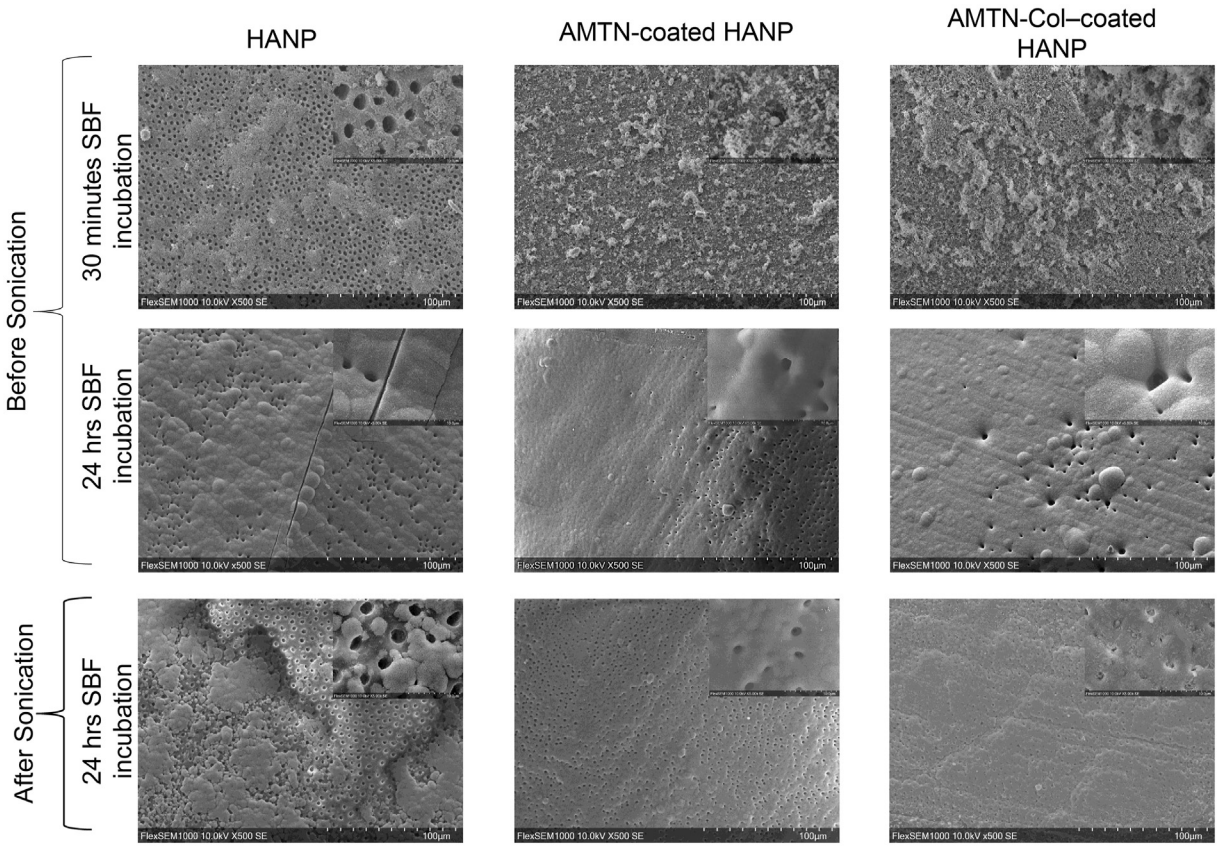

Fig. 6. SEM micrographs of totally demineralized dentin treated with AMTN/AMTN-Col–coated HANP or HANP alone, incubated with SBF for 30 min and 1 day, before and after sonication. The image inserts show a higher magnification of the same sample. Cracks are visible in HANP only treated samples after 24 h of SBF incubation. In sonicated samples, the mineral layer is mostly removed from the dentin in the HANP treated specimens, and dentinal tubules are exposed. In contrast, in the AMTN/AMTN-Col–coated HANP, the mineral layer remained intact.

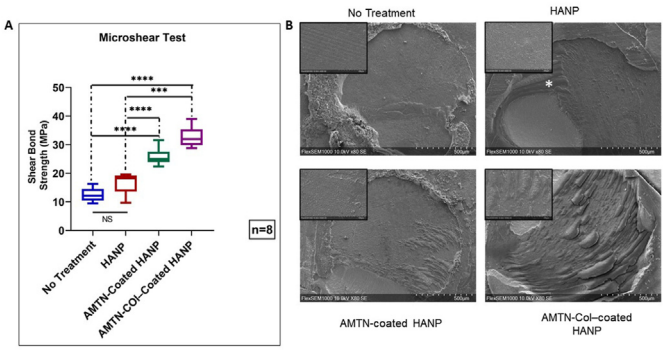

Fig. 7. (A).μSB strength for all experimental groups with 8 samples each experimental group (NS stands for non-significant) Statistical analysis was performed using one-way ANOVA and the Tukey test (***P < 0.001, ****P < 0.0001). (B) SEM micrographs of dentin-resin fracture sites after μSB tests. The asterisk in the HANP-treated sample shows an area with residual adhesive.

indicated in the Results section, samples treated with AMTN/AMTN--Col–coated HANP have shown signs of mineral formation visible to the naked eye in as low as 30 min of incubation in SBF (Fig. 5). The time is significantly lower than that observed in previous studies using non-collagenous protein for collagen mineralization [38–40]. It should be noted that measuring the effect of non-collagenous protein on collagen mineralization should be examined cautiously due to the difference in methods and materials used for studying this effect. Moving on to a more complex and clinically relevant model system, we investigated mineral formation in the presence of our bio-nano complexes on demineralized dentin sections. It has been described in several studies that dentin demineralization, either by cariogenic bacteria or during the etching step of the adhesive bonding process, activates two distinct enzymatic degradation pathways involving endogenous matrix metalloproteinases and cysteine cathepsins. The activation of these enzymes results in the auto-degradation of the denuded collagen [41,42]. In our model system, we expect these endogenous matrix metalloproteinases and cysteine cathepsins to be present in both EDTA and phosphoric acid demineralized dentin. However, their presence is more pronounced when the dentin is demineralized with phosphoric acid [43,44]. However, our findings did not show any synergistic effect between the presence of these enzymes and proteins on the mineral-promoting effect of the bio-nano complexes.

Dentin mineralization results coincided with *in vitro* collagen mineralization, with the highest degree of mineralization in the presence of the bio-nano complexes (Fig. 6). Interestingly, we had also found that the mineral layer formed in the presence of HANP alone did not integrate and was separated from dentin when a gentle, vibratory force was applied by sonication. There were no significant changes in the homogeneity of the mineral in the AMTN/AMTN-Col–coated HANP-treated group after sonication (Fig. 6). A similar method has previously been used to investigate the adhesive layer bond strength to the dentin at the dentin-resin interface using different bonding conditions [45]. Furthermore, all treated groups have shown occlusion of dentinal tubules. However, dentinal tubules remained occluded after sonication in only those samples treated with the bio-nano complexes. The occlusion of dentinal tubules is generally considered the most effective therapy for DH. Previous studies have used various agents to occlude the dentinal tubules with minerals. It was suggested that occluding dentinal tubules with minerals

could reduce DH significantly by the reduction in permeability and fluid flow through dentin [46,47]. To justify the potential clinical implications of our nano-biomolecules, AMTN/AMTN-Col–coated HANP was used as a pretreatment in bonding a restorative resin to dentin. Choosing the proper test to evaluate mechanical properties at the bonded interfaces is an ongoing debate [48]. In this study, we chose the μSBS test due to sample handling limitations as a result of the small size of the dentin disks. Furthermore, to avoid the application of any stress to the composite post and the bonded interface caused by the mould removal, we have used a perforated pasta as a mould to standardize the surface area of the composite posts across all the specimens [31]. The pasta was softened and mostly disintegrated after incubation in SBF.

Our results showed that when dentin was pretreated with AMTN/AMTN-Col–coated HANP, μSB strength values increased significantly. The SEM images suggest cohesive fracture in samples treated with nano-bio complexes and adhesive fracture in the specimens that were treated with HANP alone or that were untreated (Fig. 7). These findings may further indicate a more robust dentin-resin interface in the presence of the nano-bio complexes. To further characterize the mode of these fractures, we are considering fractography in the future.

Since odontoblasts cannot repair caries-infected dentin, restorative strategies aim to replace the infected dental tissue with materials that withstand mechanical pressure, similar to native dental tissue, while preserving tooth morphology. However, a robust and fully integrated hybrid layer is required to improve restoration longevity. Therefore, previous studies have used biomodification, such as enzyme inhibitors, collagen cross-linking, and biomimetic remineralization strategies, to preserve the collagen at the hybrid layer [36]. However, in our study, we have placed a biomineralizing agent at the interface of the dentin-restoration material that can mineralize this interface, protect the collagen, and close the gap even after the placement of the restoration. Comparing our results to similar studies, we found that the dentin-resin μSB strength value was similar to that of enamel in the specimens treated with the bio-nano complexes [49,50]. The bond to enamel is stronger than the bond strength to dentin due to the higher inorganic content of enamel compared to dentin [51]. In contrast, nontreated samples or those treated with HANP alone had a μSB value equal to that of the dentin-resin bond. This may further indicate mineralization of the dentin-resin interface in the presence of the bio-nano complexes, which led to a stronger bond similar to that of the enamel-resin bond. Further well-designed clinical studies are required to determine the potential for any clinical applications, which may also require investigating the bio-nano complexes toxicity effects on cells.

5. Conclusion

In conclusion, we have developed and characterized HANP coated with AMTN/AMTN-Col based on the high affinity of the proteins to HA. These bio-nano complexes have shown enhanced potential in mineralizing collagen, both in collagen and in dentin. Furthermore, we have demonstrated enhanced μSB strength in the dentin-resin bond following pretreatment with these bio-nano complexes. These findings may have direct implications for developing therapeutic strategies for deep dentinal caries and DH prevention.

Credit author statement

Mehrnoosh Neshatian: Conceptualization, Methodology, Investigation, Validation, Formal analysis, Visualization, Writing – original draft. Holcroft: Investigation. Anil Kishen: Conceptualization, Methodology, Writing – review& edit, Supervision, Formal analysis. Grace De Souza: Conceptualization, Methodology, Formal analysis, Writing – review& edit. Bernhard Ganss: Conceptualization, Methodology, Supervision, Formal analysis, Resources, Funding acquisition, Writing – review & edit.

Declaration of competing interest

The authors declare that they have no known competing financial interests or personal relationships that could have appeared to influence the work reported in this paper.

Acknowledgment

This project was supported by the National Sciences and Engineering Research Council of Canada (NSERC, Discovery grant RGPIN-2019-07070) to BG, the Canadian Institutes of Health Research (CIHR, operating grant MOP- 119310) to BG, (CIHR, Frederick Banting and Charles Best Doctoral scholarship, Appl#:380560) to MN. We thank Dr. Laurent Bozec (Faculty of Dentistry, University of Toronto, Canada) for his permission to use the FTIR instrument in his lab, Nancy Valiquette (Faculty of Dentistry, University of Toronto, Canada) and Jian Wang (Faculty of Dentistry, University of Toronto, Canada) for their expert assistance with the histology and mechanical testing. The graphical abstract was made using Biorender.

Appendix A. Supplementary data

Supplementary data to this article can be found online at https://doi.org/10.1016/j.mtbio.2022.100255.

References

[1] P. Gilbert, M. Abrecht, B.H. Frazer, The organic-mineral interface in biominerals, Rev. Mineral. Geochem. 59 (2005) 157–185.
[2] P. Fratzl, Collagen: Structure and Mechanics, an Introduction, Springer, Collagen, 2008, pp. 1–13.
[3] M. Maher, M. Castilho, Z. Yue, V. Glattauer, T.C. Hughes, J.A. Ramshaw, et al., Shaping collagen for engineering hard tissues: towards a printomics approach, Acta Biomater. 131 (2021) 41–61.
[4] P. Wen, M.X. Chen, Y.J. Zhong, Q.Q. Dong, H.M. Wong, Global burden and inequality of dental caries, 1990 to 2019, J. Dent. Res. (2021), 00220345211056247.
[5] R.M. Vaderhobli, Advances in dental materials, Dental Clin. 55 (2011) 619–625.
[6] M. Hannig, C. Hannig, Nanomaterials in preventive dentistry, Nat. Nanotechnol. 5 (2010) 565–569.
[7] LE Bertassoni, J.P. Orgel, O. Antipova, M.V. Swain, The dentin organic matrix–limitations of restorative dentistry hidden on the nanometer scale, Acta Biomater. 8 (2012) 2419–2433.
[8] J.L. Ferracane, Resin composite—state of the art, Dent. Mater. 27 (2011) 29–38.
[9] H. Askar, J. Krois, G. Göstemeyer, P. Bottenberg, D. Zero, A. Banerjee, et al., Secondary caries: what is it, and how it can be controlled, detected, and managed? Clin. Oral Investig. 24 (2020) 1869–1876.
[10] I. Nedeljkovic, K.L.V. Landuyt, Secondary Caries, Dental Composite Materials for Direct Restorations, Springer, 2018, pp. 235–243.
[11] J. Sabbagh, J.C. Fahd, R.J. McConnell, Post-operative sensitivity and posterior composite resin restorations: a review, Dent. Update 45 (2018) 207–213.
[12] K. Mukherjee, G. Visakan, J. Phark, J. Moradian-Oldak, Enhancing collagen mineralization with amelogenin peptide: toward the restoration of dentin, ACS Biomater. Sci. Eng. 6 (2020) 2251–2262.
[13] U.B. Mrinalini, M.N. Hegde, G.S. Bhat, An Update on Dentinal Hypersensitivity-Aetiology to Management–A Review, 2021.
[14] P. Ustriyana, F. Schulte, F. Gombedza, A. Gil-Bona, S. Paruchuri, F.B. Bidlack, et al., Spatial survey of non-collagenous proteins in mineralizing and non-mineralizing vertebrate tissues ex vivo, Bone Rep. 14 (2021) 100754.
[15] X. Xu, X. Chen, J. Li, Natural protein bioinspired materials for regeneration of hard tissues, J. Mater. Chem. B 8 (2020) 2199–2215.
[16] M. Goldberg, P. DenBesten, Y. Nakano, Extracellular Matrix Proteins: Nomenclature and Functions in Biomineralization, Extracellular Matrix Biomineralization of Dental Tissue Structures, Springer, 2021, pp. 35–51.
[17] K. Iwasaki, E. Bajenova, E. Somogyi-Ganss, M. Miller, V. Nguyen, H. Nourkeyhani, et al., Amelotin—a novel secreted, ameloblast-specific protein, J. Dent. Res. 84 (2005) 1127–1132.
[18] R.S. Lacruz, Y. Nakayama, J. Holcroft, V. Nguyen, E. Somogyi-Ganss, M.L. Snead, et al., Targeted overexpression of amelotin disrupts the microstructure of dental enamel, PLoS One 7 (2012), e35200.
[19] Y. Nakayama, J. Holcroft, B. Ganss, Enamel hypomineralization and structural defects in amelotin-deficient mice, J. Dent. Res. 94 (2015) 697–705.
[20] N. Abbarin, S. San Miguel, J. Holcroft, K. Iwasaki, B. Ganss, The enamel protein amelotin is a promoter of hydroxyapatite mineralization, J. Bone Miner. Res. 30 (2015) 775–785.
[21] I.R. Bordea, S. Candrea, G.T. Alexescu, S. Bran, M. Băciuț, G. Băciuț, et al., Nano-hydroxyapatite use in dentistry: a systematic review, Drug Metab. Rev. 52 (2020) 319–332.

[22] C.C. Coelho, L. Grenho, P.S. Gomes, P.A. Quadros, M.H. Fernandes, Nano-hydroxyapatite in oral care cosmetics: characterization and cytotoxicity assessment, Sci. Rep. 9 (2019) 1–10.
[23] G. Molino, M.C. Palmieri, G. Montalbano, S. Fiorilli, C. Vitale-Brovarone, Biomimetic and mesoporous nano-hydroxyapatite for bone tissue application: a short review, Biomed. Mater. 15 (2020), 022001.
[24] Habibah Tu, D.V. Amlani, M. Brizuela, Hydroxyapatite Dental Material, 2018.
[25] G. He, A. George, Dentin matrix protein 1 immobilized on type I collagen fibrils facilitates apatite deposition in vitro, J. Biol. Chem. 279 (2004) 11649–11656.
[26] N. Jing, A. Zhou, Q. Xu, The synthesis of super-small nano hydroxyapatite and its high adsorptions to mixed heavy metallic ions, J. Hazard Mater. 353 (2018) 89–98.
[27] M. Jung, T.K. Kim, C. Pack, J.Y. Mun, Immuno-gold Techniques in Biomedical Sciences, Advanced Imaging and Bio Techniques for Convergence Science, Springer, 2021, pp. 133–152.
[28] A. Oyane, H. Kim, T. Furuya, T. Kokubo, T. Miyazaki, T. Nakamura, Preparation and assessment of revised simulated body fluids, J. Biomed. Mater. Res. A 65 (2003) 188–195. The Japanese Society for Biomaterials, and The Australian Society for Biomaterials and the Korean Society for Biomaterials.
[29] S.N. Meloan, H. Puchtler, Chemical mechanisms of staining methods: von Kossa's technique: what von Kossa really wrote and a modified reaction for selective demonstration of inorganic phosphates, J. Histotechnol. 8 (1985) 11–13.
[30] Y. Shimada, S. Yamaguchi, J. Tagami, Micro-shear bond strength of dual-cured resin cement to glass ceramics, Dent. Mater. 18 (2002) 380–388.
[31] L.N. Ferraz, W.F.V. Júnior, G.M.B. Ambrosano, M.C.C. Giorgi, F.H.B. Aguiar, Débora Lima, Alves Nunes Leite, Effect of different concentrations of nanohydroxyapatite on tooth bleaching effectiveness and enamel bond strength, Braz. Dental Sci. 21 (2018) 17–25.
[32] Z. Sun, D. Fan, Y. Fan, C. Du, J. Moradian-Oldak, Enamel proteases reduce amelogenin-apatite binding, J. Dent. Res. 87 (2008) 1133–1137.
[33] E.J. Helmerhorst, G. Traboulsi, E. Salih, F.G. Oppenheim, Mass spectrometric identification of key proteolytic cleavage sites in statherin affecting mineral homeostasis and bacterial binding domains, J. Proteome Res. 9 (2010) 5413–5421.
[34] E.E. McDonald, H.A. Goldberg, N. Tabbara, F.M. Mendes, W.L. Siqueira, Histatin 1 resists proteolytic degradation when adsorbed to hydroxyapatite, J. Dent. Res. 90 (2011) 268–272.
[35] M. Yu, L. Wang, W. Zhang, B. Ganss, An evolutionarily conserved subdomain in amelotin promotes amorphous calcium phosphate-to-hydroxyapatite phase transition, Cryst. Growth Des. 19 (2019) 2104–2113.
[36] L. Tjäderhane, F.D. Nascimento, L. Breschi, A. Mazzoni, , ILS Tersariol, S. Geraldeli, et al., Optimizing dentin bond durability: control of collagen degradation by matrix metalloproteinases and cysteine cathepsins, Dent. Mater. 29 (2013) 116–135.
[37] L. Tjäderhane, Buzalaf Mar, M. Carrilho, C. Chaussain, Matrix metalloproteinases and other matrix proteinases in relation to cariology: the era of 'dentin degradomics, Caries Res. 49 (2015) 193–208.
[38] A.S. Deshpande, P. Fang, X. Zhang, T. Jayaraman, C. Sfeir, E. Beniash, Primary structure and phosphorylation of dentin matrix protein 1 (DMP1) and dentin phosphophoryn (DPP) uniquely determine their role in biomineralization, Biomacromolecules 12 (2011) 2933–2945.
[39] K. Mukherjee, G. Visakan, J. Phark, J. Moradian-Oldak, Enhancing collagen mineralization with amelogenin peptide: toward the restoration of dentin, ACS Biomater. Sci. Eng. 6 (2020) 2251–2262.
[40] Z. Wang, P. Ustriyana, K. Chen, W. Zhao, Z. Xu, N. Sahai, Toward the understanding of small protein-mediated collagen intrafibrillar mineralization, ACS Biomater. Sci. Eng. 6 (2020) 4247–4255.
[41] R. Seseogullari-Dirihan, F. Apollonio, A. Mazzoni, L. Tjaderhane, D. Pashley, L. Breschi, et al., Use of crosslinkers to inactivate dentin MMPs, Dent. Mater. 32 (2016) 423–432.
[42] P. Altinci, M. Mutluay, L. Tjäderhane, A. Tezvergil-Mutluay, Effect of calcium fluoride on the activity of dentin matrix-bound enzymes, Arch. Oral Biol. 96 (2018) 162–168.
[43] B.S.O. Ahmet, R. Seseogullari-Dirihan, A. Tezvergil-Mutluay, Activation of matrix-bound endogenous proteases by self-etch adhesives, Dent. Mater. J. (2020) 2019–2304.
[44] A. Tezvergil-Mutluay, M. Mutluay, R. Seseogullari-Dirihan, Ka Agee, W.O. Key, D. Scheffel, et al., Effect of phosphoric acid on the degradation of human dentin matrix, J. Dent. Res. 92 (2013) 87–91.
[45] P. Spencer, Y. Wang, Adhesive phase separation at the dentin interface under wet bonding conditions, J. Biomed. Mater. Res.: An Official Journal of The Society for Biomaterials 62 (2002) 447–456. The Japanese Society for Biomaterials, and The Australian Society for Biomaterials and the Korean Society for Biomaterials.
[46] M.G. Gandolfi, F. Iacono, C. Pirani, C. Prati, The use of calcium-silicate cements to reduce dentine permeability, Arch. Oral Biol. 57 (2012) 1054–1061.
[47] M. Toledano-Osorio, E. Osorio, F.S. Aguilera, A. Luis Medina-Castillo, M. Toledano, R. Osorio, Improved reactive nanoparticles to treat dentin hypersensitivity, Acta Biomater. 72 (2018) 371–380.
[48] A.A. El Zohairy, M.H. Saber, A.I. Abdalla, A.J. Feilzer, Efficacy of microtensile versus microshear bond testing for evaluation of bond strength of dental adhesive systems to enamel, Dent. Mater. 26 (2010) 848–854.
[49] C. Miranda, L.H. Maykot Prates, R. de Souza Vieira, MC Marino Calvo, Shear bond strength of different adhesive systems to primary dentin and enamel, J. Clin. Pediatr. Dent 31 (2007) 35–40.
[50] R.F. Rodrigues, C.M. Ramos, P.A. Francisconi, A.F.S. Borges, The shear bond strength of self-adhesive resin cements to dentin and enamel: an in vitro study, J. Prosthet. Dent 113 (2015) 220–227.
[51] A.D. Loguercio, S.K. Moura, A. Pellizzaro, K. Dal-Bianco, R.T. Patzlaff, R.H.M. Grande, et al., Durability of enamel bonding using two-step self-etch systems on ground and unground enamel, Oper. Dent. 33 (2008) 79–88.